Reaction $^3He(\pi^+,pp)p$ at $T_\pi = 350$ and 500 MeV

L. C. Smith and R. C. Minehart
Department of Physics, University of Virginia, Charlottesville, Virginia 22901

D. Ashery, E. Piasetsky, M. Moinester, and I. Navon
Raymond and Beverly Sackler Faculty of Exact Sciences, Department of Physics, Tel-Aviv University, Ramat Aviv, Israel 69978

D. F. Geesaman, J. P. Schiffer, G. Stephens, and B. Zeidman
Argonne National Laboratory, Batavia, Illinois 60439

S. Levinson, S. Mukhopadhyay, and R. E. Segel
Northwestern University, Evanston, Illinois 60201

B. Anderson, R. Madey, and J. Watson
Kent State University, Kent, Ohio 44242

R. R. Whitney
Continuous Electron-Beam Accelerator Facility, Newport News, Virginia 23606
(Received 20 January 1989)

The reaction $^3He(\pi^+,pp)p$ was measured at $T_\pi = 350$ and 500 MeV in a kinematically complete experiment. Separate contributions from two-body and three-body pion absorption are clearly seen in recoil momentum distributions. The two-body angular distributions closely follow the shape of the free $\pi d \rightarrow pp$ cross section, although the number of deuterons estimated from the two-body yield is larger than the value 1.5 expected from isospin coupling and observed previously at lower energies. Comparison with a simple impulse approximation model suggests some of the enhancement may arise from binding of the quasideuteron, although absorption on $T=1$ (pn) pairs and the higher density of ^3He may also be a factor. The strength of the three-body component falls off with bombarding energy with roughly the same slope as for the two-body component, and accounts for $\approx 45\%$ of the total absorption cross section, a larger fraction than reported previously below the (3,3) resonance. The three-body matrix element $|M_3|^2$ displays an angular dependence at both energies which is suggestive of initial-state interactions. No evidence of final-state interactions is seen.

I. INTRODUCTION

The (π^+,pp) reaction in nuclei is often described as a quasifree process, in which the pion absorbs directly on a deuteronlike (pn) pair leaving the spectator nucleus undisturbed. Although experimental data[1] exhibit many of the systematic features associated with the familiar $\pi d \rightarrow pp$ reaction, there is general agreement that the quasideuteron mechanism alone cannot account for the total pion absorption cross section.[2] This discrepancy has triggered speculation about whether more complicated multinucleon absorption modes need to be considered.

Modifications to the simple quasifree model can arise from various nuclear distortions, such as initial-state interactions (ISI) of the incoming pion and final-state interactions (FSI) of the two outgoing protons with the rest of the nucleus. Such effects result only in a redistribution of the underlying two-nucleon strength and therefore do not constitute a new absorption mechanism. Gibbs and Kaufmann[3] treated ISI and FSI effects in detail using a nucleon cascade model of pion absorption applied to the recent ^{58}Ni data of Burger *et al.*[4] but could account for only 70% of the total absorption cross section. Evidently there is still room for an absorption mechanism which involves in a fundamental way more than two nucleons.

As the number of nucleons increases, it obviously becomes more difficult to distinguish a genuine multinucleon absorption process from the more trivial case involving distorted quasifree absorption. Studies on p-shell nuclei are further complicated by the complex experimental signature exhibited by absorption on pairs having angular momentum $L=2$ with respect to the spectator nucleus.[5,6] For these reasons, a number of experiments have focused on ^3He, which has only one spectator nucleon in a relative s state. A kinematically complete measurement of the $^3He(\pi^+,pp)p$ reaction is possible by detecting in coincidence two of the three final-state protons. This permits the selection of events on the basis of the momentum transferred to the spectator proton. Absorption on three nucleons can then be defined as those events where the spectator received more momentum then available from nuclear binding. ISI and FSI effects can be calculated more reliably in the three-body system, simplifying the identification of the fundamental absorp-

tion mechanisms.

Previous coincidence experiments at LAMPF, PSI, and TRIUMF (Refs. 7-12) studied the ^{3}He$(\pi^+,pp)p$ reaction at pion kinetic energies where absorption is dominated by excitation of the $\Delta(1232)$. These experiments identified a three-body absorption component that accounts for about $25\pm10\%$ of the total absorption cross section, surprisingly large for such a light nucleus. The three-body data show no obvious signature of a reaction mechanism, and display an angular dependence that approximately follows phase space. Following previous experience with heavier nuclei, if ISI and FSI are mostly responsible for transferring momentum to the third nucleon, then this large three-body yield should be accompanied by a corresponding decrease in the observed two-body yield. However, the two-body cross sections σ_{2N} closely follow the energy and angular dependence of the $\pi d\rightarrow pp$ reaction, in agreement with the quasideuteron model. Moreover, the magnitude of σ_{2N} scales correctly according to the number of $^3S_1$ (pn) pairs in ^{3}He, i.e.,

$$N_d\equiv\frac{\sigma_{2N}}{\sigma_{\pi d\rightarrow pp}}\approx 1.5\ , \tag{1}$$

where N_d is the effective number of deuterons.

The ^{3}He data therefore imply either that ISI and FSI are negligible or that the "undistorted" (π^+,pp) cross section is larger inside ^{3}He than for the free deuteron. Either possibility is intriguing from the point of view of improving our understanding of pion absorption. For example, several theoretical models[13,14] predict an enhancement of the (π^+,pp) yield arising from absorption on a "smaller" deuteron in ^{3}He. Homma[15] has drawn similar conclusions from studies of the (γ,pn) reaction in heavier nuclei. On the other hand, if ISI and FSI turn out to be negligible, more complex three-body mechanisms must be considered, with the constraint that the three nucleons are involved in a way which does not interfere with two-nucleon absorption. Ashery[16] has proposed such a direct absorption mechanism involving a (πNN) resonance acting as a doorway. Other three-body mechanisms involve diagrams containing direct ΔN interactions or the formation of $\Delta\Delta$ pairs, about which relatively little is known.

The goal of this experiment was to extend the study of pion absorption in ^{3}He to energies above the (3.3) resonance. Because the Δ isobar plays an important role in many models of three-body absorption, it is particularly important to understand how the relationship between the two- and three-body channels changes as the probability for Δ excitation decreases. For example, the importance of pion multiple scattering increases,[17,18] which could result in stronger (ISI) effects than at lower energies. At the same time, a larger momentum transfer is required to absorb the pion, which might reveal differences between the two-nucleon wave function of the quasideuteron and the free deuteron. Finally, the increased phase space available to the $3p$ final state at higher energies makes it easier to separate the two- and three-body channels.

This paper describes measurements of the ^{3}He$(\pi^+,pp)p$ reaction made at the highest pion energies thus far: 350 and 500 MeV. Results from the (π^-,pn) measurements will appear in a subsequent paper, and results at 165 MeV are being published separately.[7] A short review of the quasideuteron model is presented in Sec. II, followed by experimental and analysis details in Secs. III and IV. Results and discussion are presented in Secs. V and VI.

II. THEORY

Consider the reaction

$$\pi^+ + {}^3\mathrm{He}\rightarrow p_1+p_2+p_3\ , \tag{2}$$

where p_1 and p_2 are detected. The three-body final state has nine kinematic variables of which only five are independent due to energy and momentum conservation. The fivefold differential cross section, expressed in terms of the experimentally measured variables $(p_1,\theta_1,\phi_1,\theta_2,\phi_2)$, is given by

$$\frac{d^3\sigma}{d\Omega_1 d\Omega_2 dp_1}=\frac{p_1^2 p_2}{(2\pi)^5 32 p_\pi m_{\mathrm{He}} E_1 E_3(1-\boldsymbol{\beta}_2\cdot\boldsymbol{\beta}_3/\beta_2^2)}|M|^2\ , \tag{3}$$

where $\beta_i=p_i/E_i$. Trivial kinematic and phase-space factors have been separated out in order to isolate the Lorentz invariant matrix element $|M|^2$. We have chosen a simple model for $|M|^2$, discussed below, which will be fitted to the data in order to estimate the two- and three-body contributions.

To simplify the analysis, we assume the two-body and three-body components add incoherently as follows:

$$|M|^2\approx|M_2|^2+|M_3|^2\ . \tag{4}$$

Later we shall see that the data largely support this assumption. Within the plane-wave impulse approximation (PWIA), the matrix element $|M_2|^2$ is represented by the Feynman diagram in Fig. 1. If the unobserved spectator proton p_3 moves in a relative s state with respect to the quasideuteron, M_2 can be factorized as[19]

$$M_2=\frac{M_{\mathrm{He}\rightarrow pd}(t)}{t-(m_{\mathrm{He}}-m_3)^2}M_{\pi d\rightarrow pp}(s,u,t)\ . \tag{5}$$

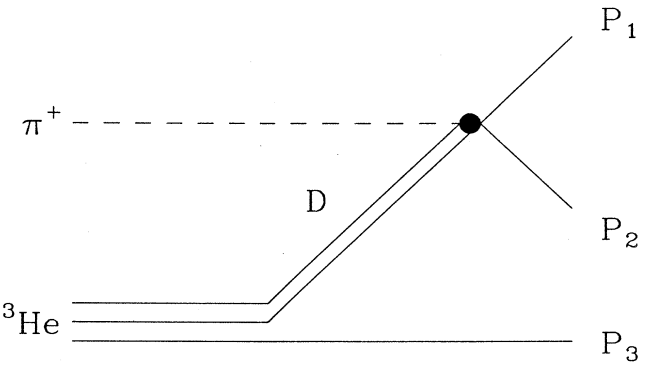

FIG. 1. Feynman diagram of quasideuteron absorption in ^{3}He. p_1 and p_2 are the detected particles, while p_3 is a spectator to the quasifree reaction.

The upper vertex in Fig. 1 represents the quasifree $\pi d \to pp$ process, given in general by an off-shell continuation of the physical absorption amplitude $M_{\pi d \to pp}$. Here we simply relate this amplitude to the free $\pi d \to pp$ c.m. cross section in the usual way,

$$\frac{d\sigma}{d\Omega_1} = \frac{1}{64\pi^2 s}\left[\frac{p_1}{p_\pi}\right]_{\text{c.m.}} |M_{\pi d \to pp}(s,u)|^2 , \quad (6)$$

where $s=(P_1+P_2)^2$, $u=(P_\pi-P_1)^2$, and the cross section is evaluated in the system where $\mathbf{p}_1+\mathbf{p}_2=0$.

The vertex function $M_{\text{He}\to pd}$ describes the virtual decay of the ^{3}He ground state into a deuteron and proton. Both $M_{\text{He}\to pd}$ and the propagator depend only on the invariant four-momentum t transferred to the virtual deuteron

$$t=(P_{\text{He}}-P_3)^2=m_{\text{He}}^2+m_3^2-2E_3 m_{\text{He}} . \quad (7)$$

In conformity with the uncertainty principle, the strongest contribution to M_2 comes when the deuteron is nearly on shell, i.e., $\sqrt{t}\approx m_d$. The resulting low relative momentum between the virtual deuteron and the recoiling proton corresponds to a large relative separation, so under these conditions the proton is expected to behave as a spectator. This purely nuclear structure component of M_2 can be calculated very accurately in ^{3}He from solutions of the three-body Faddeev equations. Nonrelativistically we have[19,20]

$$\left|\frac{M_{\text{He}\to pd}}{t-(m_{\text{He}}-m_3)^2}\right|^2 \to N_d\phi(p_3)|^2(2\pi)^9 2^3 E_{\text{He}}E_d \times E_1(2\pi)^{-6}(2E_d)^{-2} , \quad (8)$$

where $|\phi(p_3)|^2$ is the proton-deuteron relative momentum distribution (normalized to unity) and N_d is the number of deuterons. The various factors are required to retain overall Lorentz invariance.

When the deuteron is far off the mass shell, the propagator suppresses contributions from $|M_2|^2$. Because smaller (pd) separations are being probed, pion rescattering is more likely to result in all three nucleons sharing the momentum transfer. Since it is still unclear what mechanisms are important in three-body absorption, the simplest choice is to assume a constant matrix element $|M_3|^2$. This can be checked experimentally by comparing phase space with data taken at large spectator momenta, as discussed below.

Combining (6) and (8) we have

$$\frac{d^3\sigma}{d\Omega_1 d\Omega_2 dp_1} = K\left[\sum_{\substack{i\neq j\neq k=1\\ \text{cyclic}}}^{3} |M_2(p_i,p_j;p_k)|^2 + |M_3|^2\right] \quad (9)$$

with

$$|M_2(p_i,p_j;p_k)|^2 = 32(2\pi)^5 E_d(p_k)^{-1}E_k m_{\text{He}} \times N_d|\phi(p_k)|^2 s_{ij}\left[\frac{p_\pi}{p_i}\frac{d\sigma}{d\Omega_i}\right]_{\text{c.m.}_{ij}} , \quad (10)$$

where $E_d(p_k)=(p_k^2+m_d^2)^{1/2}$ is the energy of the quasideuteron and K is the kinematic factor multiplying $|M|^2$ in (3). Note that, in general, it is necessary to include the possibility that one of the detected particles, either 1 or 2, was the spectator.

In this paper we represent $|\phi(p)|^2$ by the two-body breakup part of the ^{3}He spectral function calculated by Meier-Hajduk *et al.*,[21] which agrees well with (pd) relative momentum distributions extracted from ^{3}He($e,e'p$)d measurements.[22] We have interpolated the energy and angle dependence of $d\sigma/d\Omega$ from previous $\pi d \to pp$ measurements[23] made in the energy region covered by this experiment. The only adjustable parameters are N_d and $|M_3|^2$ which are fitted to the data. Finally, in order to illustrate more transparently the transition between two- and three-body processes, the data are presented as recoil momentum distributions by rebinning the data in terms of the volume element $d\mathbf{p}_3$ instead of $d\Omega_2 dp_1$. The two volume elements are related by a simple Jacobian transformation.

III. EXPERIMENT

The ^{3}He(π^+,pp)p reaction was studied in the high-energy pion channel (P^3E) at LAMPF using the coincidence setup shown schematically in Fig. 2. The pion beam was incident on a cryogenic liquid-^{3}He target. Protons emitted from the target were momentum analyzed by the Large Acceptance Spectrometer (LAS), while on the opposite side of the beam line a movable array of 11 plastic scintillation counters measured the angular position, time of flight (TOF), and energy loss of particles detected in coincidence. This information was sufficient to permit identification of the 3p final state.

The LAS spectrometer has been described in detail elsewhere.[24] A valid LAS event consisted of a coincidence between the plastic scintillator $S1$ at the entrance

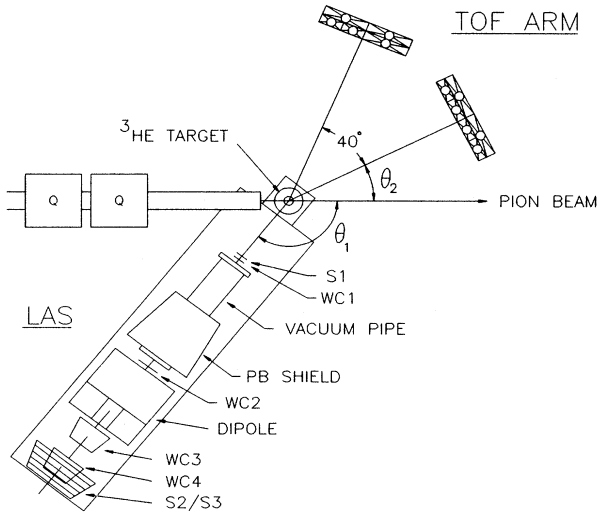

FIG. 2. Floor plan of experiment. Large acceptance spectrometer measured $\mathbf{p}_1$ while $\mathbf{p}_2$ was detected in coincidence by one of the 11 TOF counters.

of LAS and a hodoscope array $S2$ and $S3$ at the exit. Multiwire proportional chambers (MWPC) before and after the dipole magnet provided x-y coordinates used to determine the particle momentum p_1. Time of flight and momentum were used to calculate the particle mass, a typical spectrum of which is shown in Fig. 3. The two front wire chambers (WC1 and WC2) were also used to calculate the angles θ_1 and ϕ_1, and to trace the particle trajectory back to the target. Individual MWPC efficiency was usually $>95\%$ except for the front chamber WC1, which was subjected to higher rates. For this chamber 70% was more typical.

For this experiment LAS was modified to allow a larger range of scattering angles by removing the quadrupole magnets and increasing the distance from the target to WC1. This reduced the solid angle from 25 to ≈ 5 msr but simplified the momentum calculation and extended the momentum bite $\delta p/p$ limits to $(-25\%, +50\%)$. The spectrometer acceptance function was determined empirically by filling the spectrometer phase space with protons from various inelastic and elastic reactions. The shape did not deviate more than 3% from the calculated acceptance, using the program TURTLE.[25] Momentum resolution within the acceptance was typically 2% (FWHM), and momentum centroid errors were typically 1%.

Detection of a second particle in coincidence with the one observed in LAS was accomplished with two arrays of scintillator bars[26] made of NE-102. Each array was 2 m from the target and was 1 m square, subtending an angle of $\pm 14°$ both vertically and horizontally ($\Delta\Omega = 235$ msr). One of the two arrays, called the quasifree arm, was set to an angle corresponding to 180° away from LAS in the πNN center of momentum frame in order to observe the two-body component of the absorption cross section. It was composed of a front layer of four narrow bars (each $10.16 \times 25.4 \times 101.6$ cm^3) and a back layer of two wide bars ($10.16 \times 50.8 \times 101.6$ cm^3). The other TOF array was placed 40° away from the quasifree angle to provide coverage of three-body processes. This arm was identical to the quasifree arm except that two of the narrow bars were replaced by a wide bar.

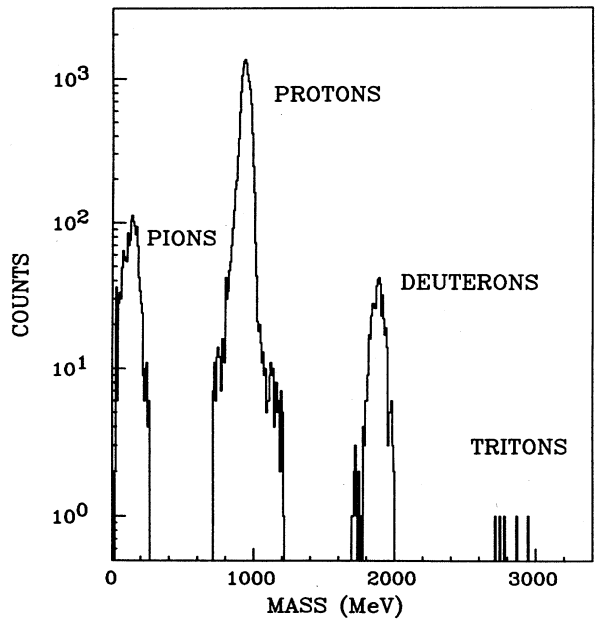

FIG. 3. Particle mass identification in LAS calculated from momentum and time of flight of p_1.

Both ends of each bar were fitted with tapered acrylic plastic light pipes coupled to Amperex XP2041 12.7 cm diameter photomultiplier tubes (PMT) surrounded by 15.2 cm diameter Ortec magnetic shields. Timing signals from each end were individually digitized and averaged to provide the mean time of arrival of the particle striking a bar. The bar time-to-digital converters (TDC's) were started by a signal derived from the coincidence particle in LAS, so it was necessary to correct for the TOF from the target to $S1$. This correction resulted in an overall TOF resolution of 1.4 nsec (FWHM). The time difference between the signals at the two ends of each bar gave the vertical position of the particle to within 10 cm (FWHM). Together with the position of the struck bar, this provided some (θ_2, ϕ_2) information.

A valid bar event consisted of a coincidence between the top and bottom PMT's of any of the 11 bars. Finally, a coincidence between LAS and one of the bars was demanded within a 60 nsec timing window. This window was more than adequate to cover the physical TOF region and extended beyond this region in order to allow estimation of accidentals. Standard CAMAC electronic apparatus, controlled by the LAMPF Q system, was used for data acquisition.

Liquid ^{3}He was maintained at a temperature of 1.5 K in a vertical target cell in thermal contact with a pumped bath of superfluid liquid ^{4}He, using a vacuum cryostat described elsewhere.[27] The cell was a 7.62-cm tall $\times$ 5.4-cm diameter cylinder with 40-mg/cm^2 stainless steel walls. Nominal target thickness at 1.5 K was 404 mg/cm^2, determined from the liquid-^{3}He vapor pressure and x-ray photographs of the target cell. The pion beam profile was found from exposing Polaroid film at the target position and was averaged over the shape of the target cell to give an average target thickness of 400 mg/cm^2 $\pm 3\%$, for which the error is due largely to beam steering uncertainties. Emptying the target cell was impractical, so an identical empty cell with four times the wall thickness (to increase the coincidence rate) was constructed to estimate the background. The cryostat was raised out of the beam in order to position the empty target cell or other solid targets in the beam.

The pion flux (averaged over the 8% LAMPF duty factor) ranged from 10^6 to 10^7 sec^{-1} with a momentum spread $\delta p/p$ of 0.5–1.0 %. Various relative monitors used to measure the beam intensity included a muon halo detector, the pion production target current toroid and an Ar-CO_2 ion chamber placed in the beam. These usually agreed to within a few percent. These monitors were calibrated periodically against the ^{2}H(π^+, pp) and ^{1}H$(\pi^+, \pi^+ p)$ reactions using CD_2 and CH_2 targets, respectively. A coincidence between a pion or proton in LAS and a proton in one of the TOF bars was demanded,

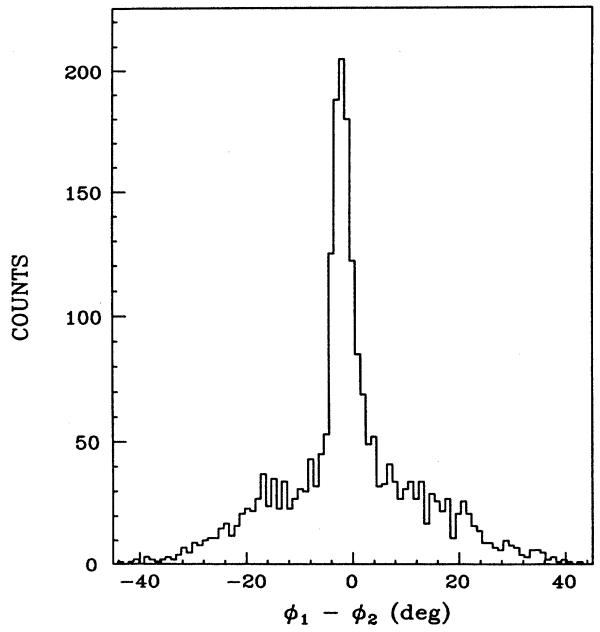

FIG. 4. Azimuthal angular correlation between p_1 and p_2 using a CD_2 target and incident π^+ beam at 350 MeV. Narrow peak identifies $\pi d \rightarrow pp$ reaction.

and the measured azimuthal angular correlation $\phi_1 - \phi_2$ between the two particles (Fig. 4) was used to distinguish the two-body yield from the largely uncorrelated quasielastic carbon background. A ^{12}C target was also used independently for background subtraction. Pion decay corrections in LAS were estimated using TURTLE.

The ^{3}He cross sections presented here were normalized relative to the $\pi d \rightarrow pp$ measurements made during this experiment. Both measurements used identical detector configurations, which largely canceled any angular or acceptance dependent systematic effects, and permitted a more direct test of the quasideuteron model. The $\pi d \rightarrow pp$ runs were in turn normalized to the parametrization of Bystricky *et al.*,[28] and additional partial-wave information was obtained from interpolation of Legendre polynomial fits to data in Ref. 23. In practice, the quantity $N_\pi \Delta\Omega_1$ was determined from each normalization run and used to calibrate the monitors. The normalization error, including target thickness and efficiency uncertainties, was $\approx$7% at 350 MeV and $\approx$9% at 500 MeV. Errors associated with the cross-section parametrization are not included.

IV. DATA ANALYSIS

Data were taken at the kinematic settings listed in Table I. LAS was set to the desired angle θ_1 with its momentum bite was centered on the value of p_1 given by $\pi d \rightarrow pp$ kinematics. With θ_1 and ϕ_1 restricted by the LAS solid angle, the coincidence yield arising from the ^{3}He(π^+,pp)p reaction could be measured as a function of p_1, θ_2, and ϕ_2, or equivalently, the recoil momentum vector $\mathbf{p}_3$.

TABLE I. Detector settings for LAS and TOF array. Two entries for θ_2 refer to quasifree and non-quasifree arms. For each angle, p_1(min) is the lowest momentum used in the analysis due to proximity to the LAS acceptance cutoff, while p_1(max) is roughly the upper limit imposed by three-body kinematics.

θ_1 (deg)	θ_2 (deg)		p_1(min,max) (MeV/c)
	350 MeV		
20	86–114	126–154	443–975
40	54–82	94–122	429–950
60	28–56	68–96	403–900
75	52–80	92–120	379–850
90	39–67	79–107	379–800
110	25–53	65–93	335–750
130	12–40	52–80	320–700
	500 MeV		
40	48–76	88–116	526–1125
60	63–91	103–131	530–1050
75	48–76	88–116	500–975
90	35–63	75–103	460–925
110	21–49	61–89	420–850

A. Identification of absorption reaction

It was necessary to distinguish the three-proton final state from various other three- and four-body final states arising from the ^{3}He($\pi,\pi' p$)d and ^{3}He($\pi,\pi' p$)pn breakup reactions. Good particle identification was therefore required (in addition to overdetermined kinematics) in order to fix the missing mass. Although our particle identification in LAS was excellent, there were some ambiguities between pions and protons in the TOF arm which are discussed shortly.

Raw data from typical runs at 350 MeV are shown in Fig. 5, where the TOF of the particle striking the TOF arm is plotted against the momentum of the proton detected in LAS. The curves labeled "3P" in Fig. 5 identify the final state having three protons and are calculated for the angle pairs listed in each plot, while the other curves are discussed below. The absorption events are distributed along this kinematic curve due to Fermi motion of the quasideuteron, and broadened in other directions to a lesser extent from the LAS momentum and bar TOF resolution, as well as from kinematic shifts arising from summing over several TOF bars. Selection of the (π^+,pp)p reaction was made by placing a cut of varying width around the (p_1, TOF_2) kinematic curve, which was recalculated for every event using the measured values of ($\theta_1,\phi_1,\theta_2,\phi_2$). Although equivalent to a missing mass cut, this procedure compensated for the fact that the missing mass resolution is not constant in a TOF measurement.

Also visible in Fig. 5 are strong enhancements in the kinematic region for quasifree proton knockout, where the backscattered pion struck a TOF bar after knocking the proton into LAS. These events are clustered along the lowest curves in Fig. 5, which describe the (π,p,d)

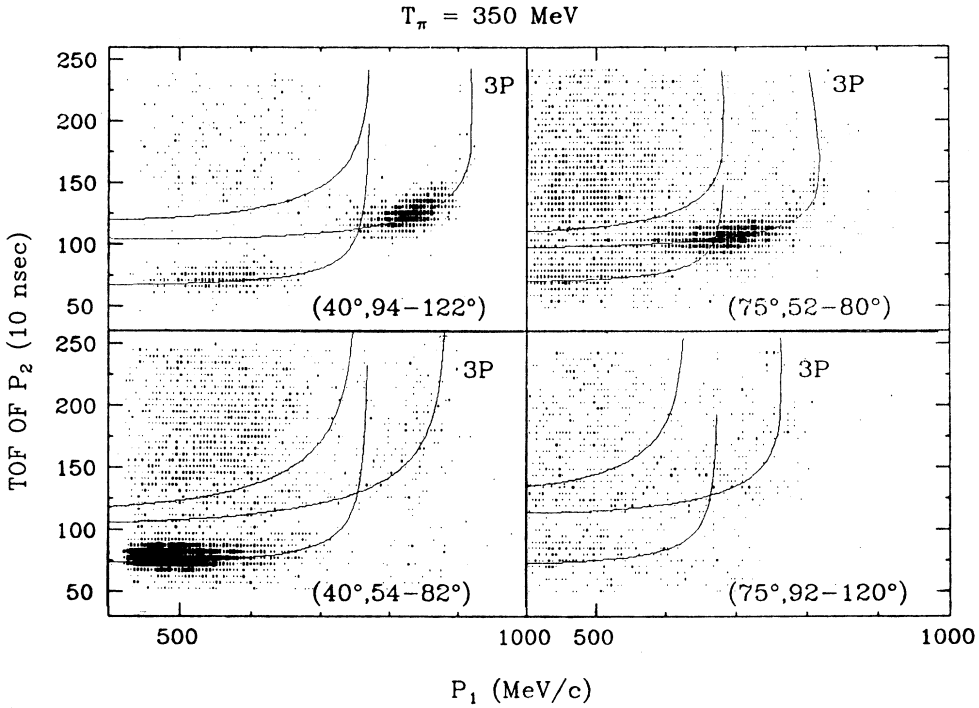

FIG. 5. Typical coincidence data for 350 MeV pions incident on ^{3}He target. (θ_1,θ_2) refer to central angles of LAS and TOF arm, respectively. For upper plots LAS and TOF arm were set to $\pi d \rightarrow pp$ kinematics; for lower plots TOF arm was 40° away. Events from individual bars in TOF arm have been summed together. Curves labeled "3*P*" denote ^{3}He$(\pi^+,pp)p$ events and were calculated for the particular angles shown, assuming $\phi_1=180°$ and $\phi_2=0°$. Other curves are described in the text.

final state. As some of these pions can have the same TOF as absorption protons, such (π,p) coincidences could be counted as absorption events. Fortunately, contributions from the knockout reaction are largely suppressed within the absorption cut by the proton momentum distribution in ^{3}He. Pions that do fall inside the cut are low enough in energy (<70 MeV) to stop in the front bars, and are distinguished from the more energetic protons in this region by demanding a coincidence between the front and back counters.

Events lying above and to the left of the uppermost curve in Fig. 5 populate four-body phase space and consist mostly of (p,p) and (p,n) coincidences arising from the ^{3}He$(\pi^+,\pi^+p)pn$ breakup reaction. This is evidence of strong pion multiple scattering and has been reported previously at high energies in (π,π') measurements by Boswell *et al.*[17] and Klein *et al.*[18] Later we discuss the implications of two-nucleon knockout in the present measurement with respect to the mechanism of three-nucleon absorption in ^{3}He.

B. Calculation of recoil cross sections

Events satisfying the absorption cut are plotted in Fig. 6 as a function of p_1, θ_2, and ϕ_2 for $\theta_1=75°$. Only coincidences from the quasifree TOF arm are shown. Superimposed on each distribution is a curve showing the kinematic dependence of the momentum p_3 of the undetected proton (calculated by fixing the other two variables at their quasifree values). The peaking around $p_3=0$ clearly reveals the quasifree nature of the reaction, and demonstrates that the physics is more economically presented using p_3 as the independent variable.

Accordingly, absorption events from both TOF arms were combined and rebinned into histograms containing the calculated recoil momentum. Before binning, each event was weighted appropriately to account for LAS acceptance, wire chamber efficiency and electronic dead time. The combination of acceptance cutoffs and straggling in the target prevented protons having momenta <250 MeV/c from being detected in either arm. Somewhat higher thresholds were used in the analysis to avoid large corrections arising from the LAS acceptance function or large corrections to the measured TOF from energy loss in the target. Table I summarizes the cuts on p_1 determined by the LAS acceptance. Accidentals were estimated using events that lay outside of the physical time-of-flight region by shifting them either forward or backward in time, then performing the identical analysis procedure as for the reals. The empty target runs were treated similarly. Most of the error associated with the calculated kinematic variables was due to the coarse horizontal resolution of the TOF arm. To smooth over this error the x coordinate in each struck bar was randomly chosen before (θ_2,ϕ_2) was calculated. This prevented artificial structure from appearing in the various distribu-

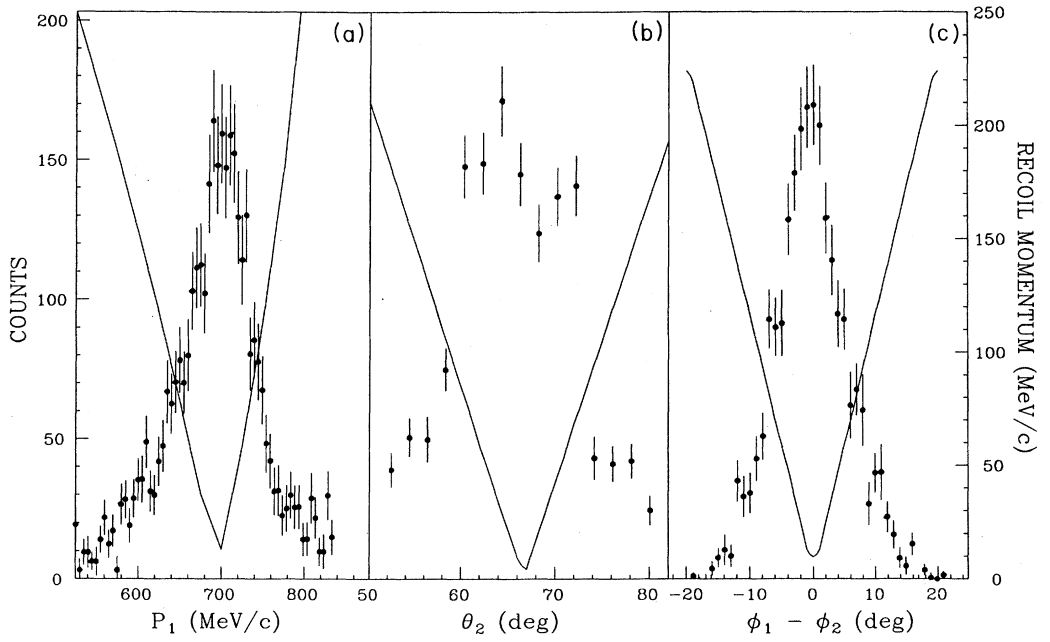

FIG. 6. Distribution of ^{3}He(π^+,pp)p events at 350 MeV as a function of the measured variables p_1, θ_2, and $\phi_1-\phi_2$, with $\theta_1=75°$. Overall θ_2 resolution in (b) is 5°. Solid curve shows dependence of recoil momentum p_3 on these variables. Peaking around $p_3=0$ is evidence of quasifree two-body absorption.

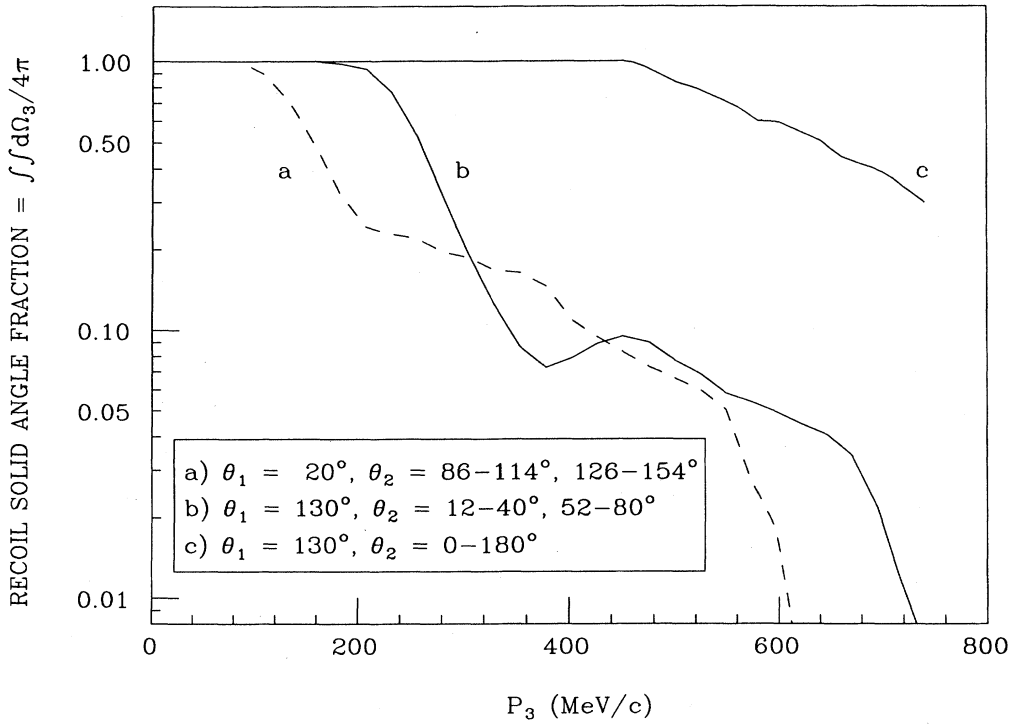

FIG. 7. Recoil momentum volume element $\Delta\Omega_3$ (normalized to 4π) used in expression (12) to define the cross section, calculated using Monte Carlo simulation of experiment. Typical result shown for 350 MeV illustrates how various detector configurations limit the direction of $\mathbf{p}_3$ at large recoil momenta (curves a,b). Even if no acceptance limits are placed on p_1, θ_1, or ϕ_2 (curve c), momentum conservation ultimately restricts the direction of $\mathbf{p}_3$.

tions. The overall recoil momentum resolution was $\sigma_{p_3} \approx 25$ MeV/c, $\sigma_{\theta_3} \approx 10°$ and $\sigma_{\phi_3} \approx 15°$.

The number of events, $N(p_3)$, in each p_3 bin is defined in terms of the recoil differential cross section by

$$N(p_3) = N_\pi N_t \int\int_{\Delta p_3}\int\int\int \frac{d^2\sigma}{d\Omega_1 d\mathbf{p}_3} d\Omega_1 p_3^2 dp_3 d\Omega_3 , \tag{11}$$

where N_t is the number of target nuclei cm^{-2} and N_π is the number of pions incident on the target. The domain of integration over the direction of $\mathbf{p}_3$ is, of course, constrained by the limitations imposed on $\mathbf{p}_1$ and $\mathbf{p}_2$ by the detector acceptances. As shown below, this makes it impossible to study the complete dependence of $d^2\sigma$ on θ_3 and ϕ_3 for $p_3 \geq 200$ MeV/c, where our experimental statistics are anyhow limited. Since we do not expect the cross section to depend strongly on these variables, we calculate the average cross section in each p_3 bin according to

$$\frac{d^2\sigma}{d\Omega_1 d\mathbf{p}_3} \equiv \frac{N(p_3)}{N_t N_\pi \Delta\Omega_1 p_3^2 \Delta p_3 \Delta\Omega_3} . \tag{12}$$

The recoil solid angle $\Delta\Omega_3$ was calculated for each p_3 bin using a Monte Carlo simulation of the experiment. We show the calculated $\Delta\Omega_3$ (normalized to 4π) in Fig. 7 for two kinematic configurations, corresponding to the smallest ($\theta_1 = 20°$) and largest ($\theta_1 = 130°$) LAS settings used. We also show the total available recoil solid angle $\Delta\Omega_3^{\max}$ obtained by integrating beyond the physical acceptances of the detectors (but with θ_1 and ϕ_1 fixed). Generally speaking, for small values of $\mathbf{p}_3$, there is no constraint on its direction imposed by the apparatus, so the $d\mathbf{p}_3$ volume element is sampled uniformly over 4π steradians. As the magnitude of $\mathbf{p}_3$ increases, its direction is confined by conservation of momentum to lie in the scattering plane defined by LAS and to point more in the direction of the incident pion, causing first $\Delta\Omega_3$ and eventually $\Delta\Omega_3^{\max}$ to decrease below 4π. As Fig. 7 demonstrates, this constraint means more complete recoil solid angle coverage was provided when the large area TOF counters were at forward angles.

V. RESULTS

The measured recoil distributions are plotted in Figs. 8 and 9 for $T_\pi = 350$ and 500 MeV, respectively. The data

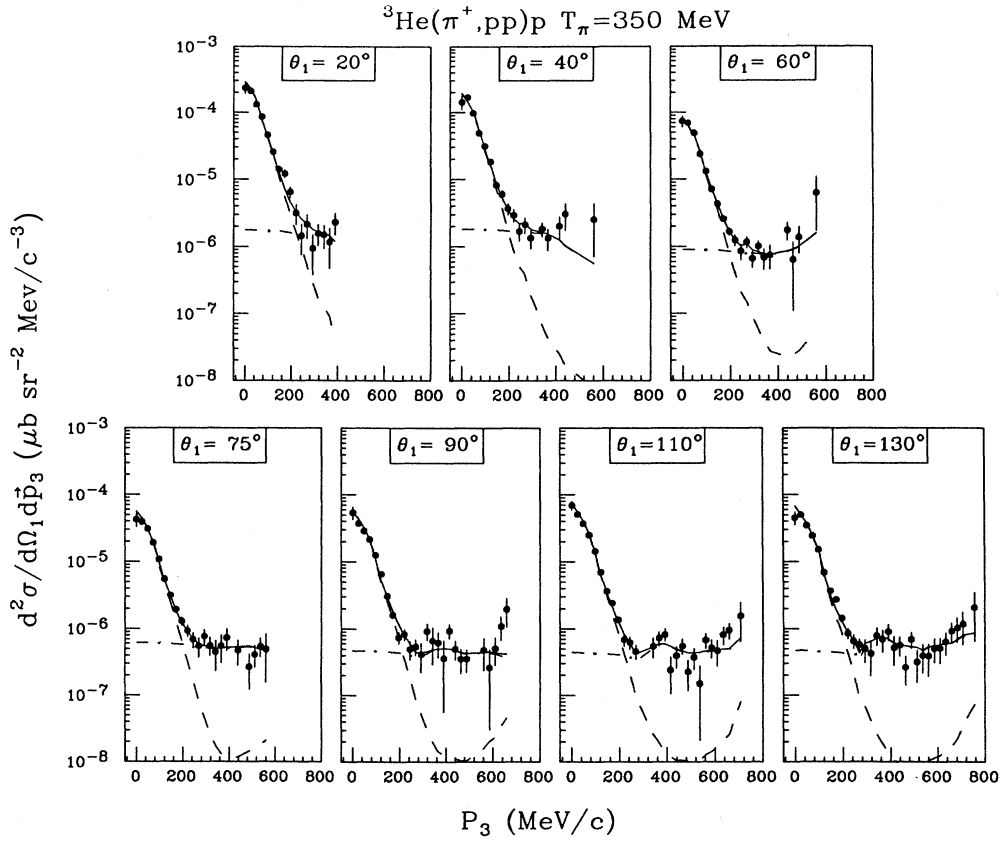

FIG. 8. Recoil momentum distributions $d^2\sigma/d\Omega_1 d\mathbf{p}_3$ of ^{3}He(π^+,pp)p at 350 MeV. Units are (μb sr^{-2} MeV/c^{-3}). Cross sections have been averaged over the direction of $\mathbf{p}_3$. LAS angle θ_1 is in the lab frame. Dashed line: PWIA calculation of $|M_2|^2$; dot-dashed line: constant matrix element $|M_3|^2$. Calculations have been normalized to data using fitting factors N_d^{PWIA} and $|M_3|^2$ given in Table II.

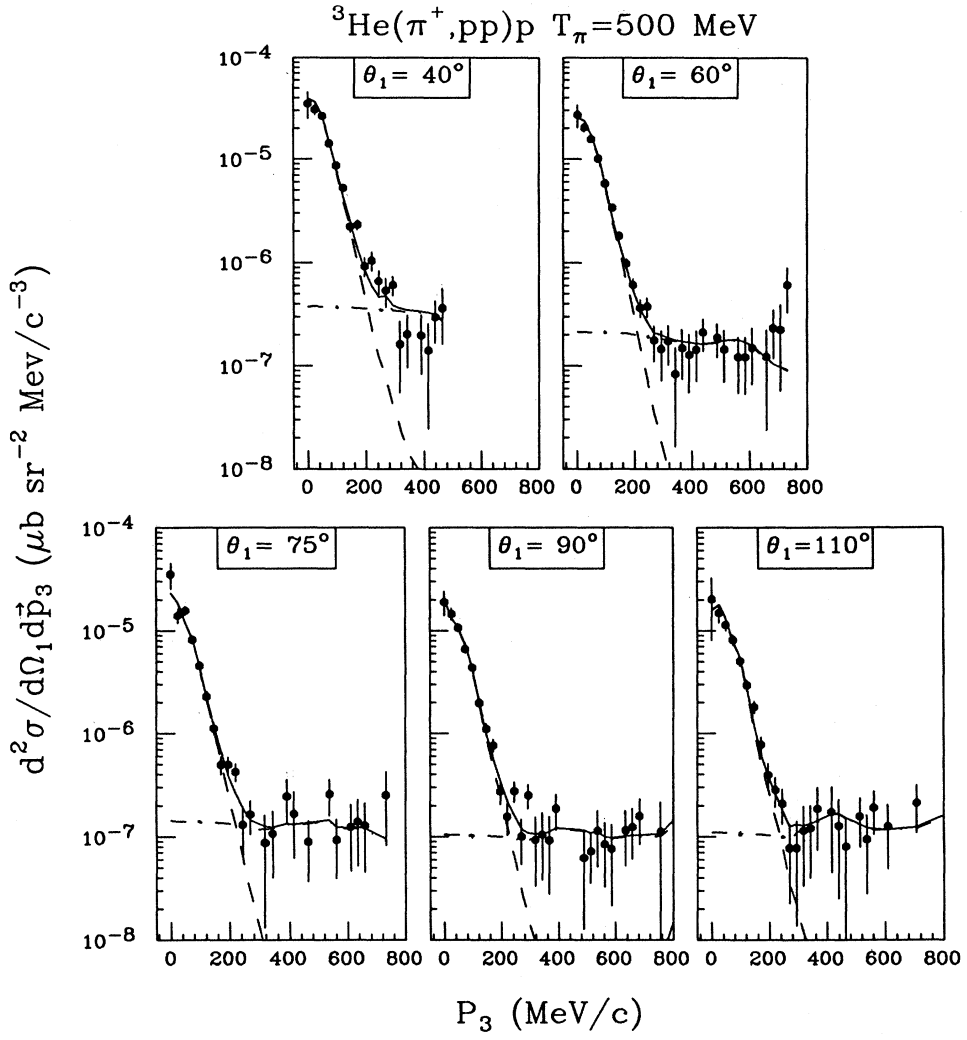

FIG. 9. Same as Fig. 8 at 500 MeV.

points were calculated from (12) and show statistical error bars only. The solid curve shows the theoretical cross section obtained from integrating (3) over the angular and energy acceptance of the apparatus and adjusting the constants N_d and $|M_3|^2$ [defined in (4) and (8)] to fit the data at each θ_1 setting. The integration was performed using a Monte Carlo computer program which took into account the kinematic resolution of the detectors. The fitted two- and three-body contributions are indicated by the dashed and dot-dashed lines, respectively. Results are tabulated in Table II.

The signature of quasifree absorption on a (pn) pair is evident from the strong dependence of the measured cross section on the momentum p_3 of the recoiling proton. No significant deviation from the shape predicted by the PWIA matrix element $|M_2|^2$ is seen, indicating the momentum distribution of the (pn) pair is well described by the theoretical (pd) spectral function for recoil momenta up to ≈ 200 MeV/c. At higher values of p_3, for which it is a poorer approximation to treat the recoil nucleon as a spectator, the PWIA curve grossly underestimates the yield and the data more or less follow three-body phase space. The large error bars in this region reflect the residual statistical uncertainty after subtracting accidentals, which contributed $\approx 50\%$ of the events involving large recoil momenta.

The distinct separation between two-body and three-body processes on the basis of recoil momentum makes it feasible to attempt to estimate the "cross section" for each component. This approximation of treating the two amplitudes incoherently is made more plausible by the absence in the data of any obvious interference effects in the region around $p_3=200$ MeV/c where $|M_2|^2 \approx |M_3|^2$.

A. Two-body absorption

The differential cross sections for two-body absorption were obtained directly from the recoil momentum distributions after first subtracting the underlying three-body background. This background was assumed to follow the

TABLE II. Results of PWIA and phase-space fits to recoil momentum distributions taken at the kinetic settings in Table I. Errors are statistical only. N_d^{PWIA} normalizes the (pd) momentum distribution used in $|M_2|^2$ and is the effective number of deuterons consistent with the PWIA calculation. $|M_3|^2$ normalizes the integrated phase space K accepted by the detectors. Extracted cross sections are given in the laboratory frame. $N_d^{\mathrm{exp}} \equiv d\sigma_{2N}/d\sigma_{\pi d}$ empirically defines the effective deuteron number, where $d\sigma_{\pi d}$ is the free $\pi d \rightarrow pp$ cross section. The three-body cross section is given by $d\sigma_{3N} = |M_3|^2 \int K d\mathbf{p}_3$ and the values given for the phase-space integral $\int K d\mathbf{p}_3$ are normalized to $|M_3|^2 = 1$.

θ_1 (deg)	N_d^{PWIA}	$\lvert M_3\rvert^2$ ($\times 10^9$)	χ^2	$d\sigma_{2N}/d\Omega_1$ (μb/sr)	N_d^{exp}	$\int K d\mathbf{p}_3$ (μb/sr)	$d\sigma_{3N}/d\Omega_1$ (μb/sr)
				350 MeV			
20	1.40(4)	1.26(20)	1.5	1009(38)	1.71(6)	1540	1940(308)
40	1.42(4)	1.52(17)	1.8	630(28)	1.70(7)	1322	2009(225)
60	1.50(4)	0.90(8)	0.7	284(11)	1.71(7)	1148	1033(92)
75	1.47(4)	0.74(7)	1.6	220(10)	1.72(8)	968	716(68)
90	1.35(4)	0.69(7)	2.0	222(8)	1.60(6)	813	561(57)
110	1.36(4)	0.81(6)	1.6	282(10)	1.60(6)	639	517(38)
130	1.35(4)	1.05(8)	1.8	285(12)	1.53(6)	535	562(43)
				500 MeV			
40	1.44(5)	0.36(4)	2.7	200(10)	1.81(9)	1711	616(68)
60	1.77(5)	0.25(3)	1.3	114(4)	1.94(7)	1373	343(41)
75	1.66(7)	0.21(4)	1.2	90(4)	1.89(8)	1151	242(46)
90	1.67(7)	0.19(3)	1.0	87(4)	1.91(9)	934	177(28)
110	1.81(9)	0.26(4)	1.0	99(5)	1.94(10)	735	191(29)

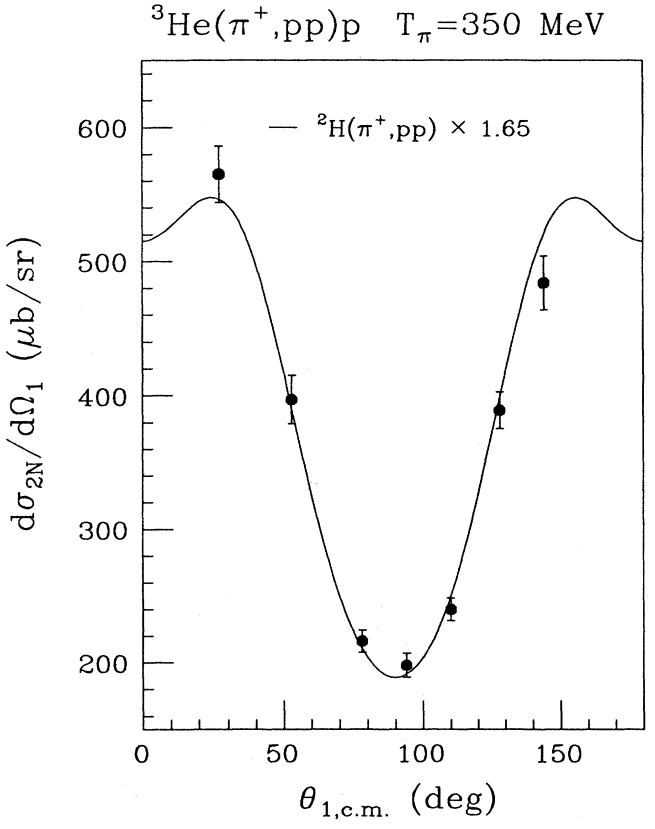

FIG. 10. Angular distribution of two-body absorption yield in ^{3}He at 350 MeV plotted in πd c.m. system. Solid line shows free $\pi d \rightarrow pp$ cross section multiplied by the indicated scale factor to fit the data.

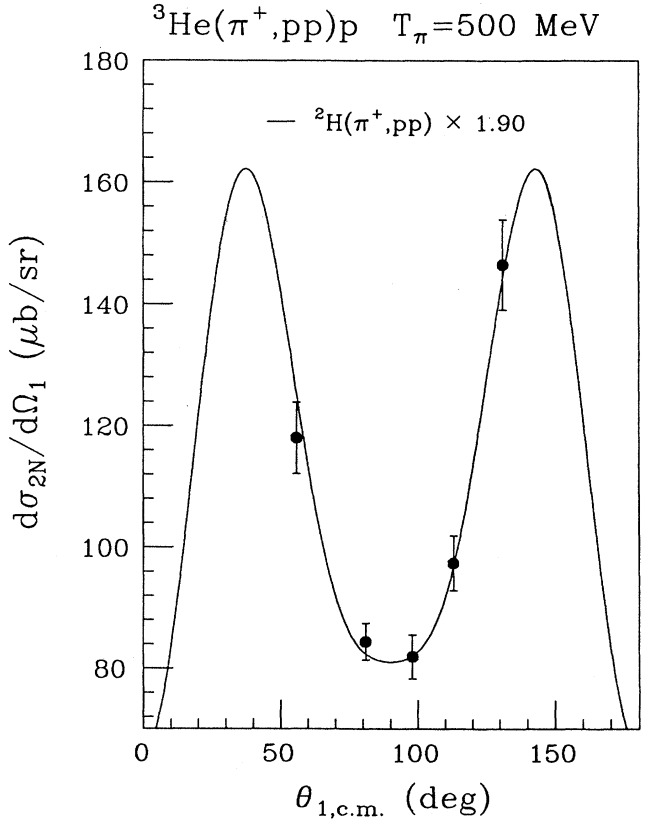

FIG. 11. Same as Fig. 10 at 500 MeV.

phase-space shape shown in Figs. 8 and 9, which was normalized to the data using the fitted values of $|M_3|^2$ obtained at each angle θ_1. The resulting two-body yield was then integrated over the spectator volume element $d\mathbf{p}_3 \approx 4\pi p_3^2 dp_3$, yielding the values of $d\sigma/d\Omega_1$ summarized in Table II. Also listed for each angle is the effective number of deuterons $N_d^{\rm exp}$, defined as the ratio of the ^{3}He two-body cross section to the free $\pi d \to pp$ cross section. At 500 MeV these ratios exceed by 30% the quasideuteron value of 1.5 observed at lower energies.[11] Possible explanations for an enhanced quasideuteron yield are discussed in Sec. VI.

The two-body cross sections, transformed to the c.m. frame using the standard $\pi d \to pp$ Jacobian, are plotted in Figs. 10 and 11. For comparison, the free $\pi d \to pp$ c.m. angular distributions at 350 and 500 MeV are shown scaled to the data. The scale factors at each energy were obtained by averaging the values of $N_d^{\rm exp}$ in Table II. The symmetry about 90° observed in the ^{3}He data gives us confidence in our subtraction of the three-body background. Furthermore, the observed similarity between the ^{3}He and ^{2}H angular distributions strongly suggest an undistorted quasideuteron mechanism. Because data at small c.m. angles were not obtained, we could not verify whether the ^{3}He angular distribution exhibited the same bending over seen in the $\pi d \to pp$ reaction at these energies. This makes somewhat ambiguous the use of a Legendre polynomial fit to determine the total two-body absorption. We choose instead to define σ_{2N} relative to $\sigma_{\pi d}$ using the scale factors determined for each energy. This gives σ_{2N}(350 MeV)=2.19±0.09 mb, and σ_{2N}(500 MeV)=0.72±0.02 mb, where the errors are statistical only.

B. Three-body absorption

The θ_1 dependence of the fitted three-body matrix elements $|M_3|^2$ is plotted in Fig. 12 (left-hand side). A pronounced angular dependence is seen which is symmetric about 90° in the lab frame. A Legendre polynomial fit shows the strength of the θ_1 dependent term is the same (about 60%) at both 350 and 500 MeV. Some angle dependent deviations from phase space were seen in the TRIUMF data[11] at 62.5 and 82.8 MeV, although at 120 MeV PSI data[8] showed a constant matrix element. We could find no systematic effect which would account for this feature. Although the symmetry of $|M_3|^2$ in the lab frame may seem disturbing, it is only the total absorption matrix element $|M|^2$ which must be symmetric in the three-body c.m. frame. Furthermore, since we are sampling only about 10% of the recoil phase space available at each θ_1 setting (recall Fig. 7), the fitted $|M_3|^2$ values are not necessarily representative. For example, a different choice of angle settings for the TOF arm might lead to a different angular dependence for $|M_3|^2$. Therefore, any physical interpretation of the particular angular dependence observed in Fig. 12 must take into account the effects of the truncated phase space.

From the previous discussion it is obvious that estimating the total three-body cross section from our limited sample requires a sizable extrapolation into unmeasured portions of phase space. Since we are assuming that all of

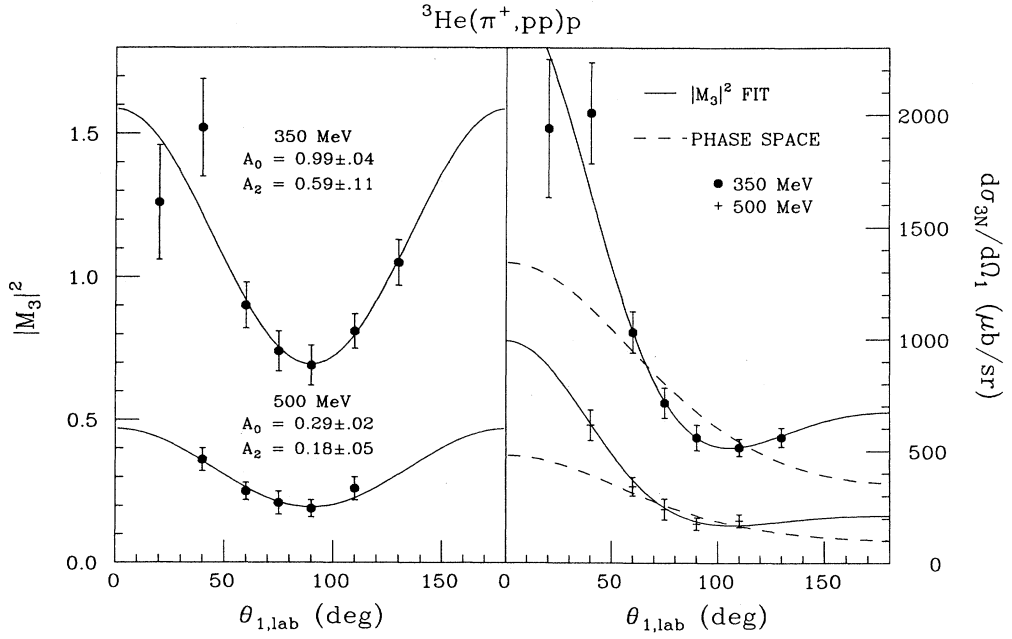

FIG. 12. Left: Lab frame angular distribution of experimentally extracted three-body matrix elements $|M_3|^2$ listed in Table II. The Legendre polynomial fit is only to guide the ey. Right: extrapolated three-body cross sections estimated from $|M_3|^2$. Results of Legendre fit are used to interpolate between plotted points (solid line). Dashed curve shows dependence of phase space, normalized to produce best fit to data around 90°. A lower limit on σ_{3N} was obtained from the integral over the phase-space curve.

TABLE III. Summary of energy dependence of two- and three-body pion absorption in ^{3}He. For this work we used the angle-averaged values of N_d^{exp} given in Table II to obtain σ_{2N}. Errors include normalization uncertainties.

$T\pi$ (MeV)	σ_{2N} (mb)	σ_{3N} (mb)	$\sigma_{3N}/\sigma_{2N+3N}$	Ref.
37.0	8.3(6)	3.4(3)	0.29(3)	12
62.5	10.2(4)	3.6(4)	0.26(3)	11
82.8	13.4(1.2)			11
120		3.9(5)		8
165	16.4(1.8)			7
350	2.19(19)	1.53(27)[a]	0.41(8)	This work
		1.80(16)[b]	0.45(5)	
500	0.72(7)	0.51(8)[a]	0.41(7)	This work
		0.64(8)[b]	0.47(7)	

[a] Using phase-space fit to $\theta_1 > 40°$.
[b] Using $|M_3^{fit}|^2$.

the (θ_3,ϕ_3) dependence of $d\sigma_{3N}$ is determined by the phase-space factor K, we have

$$\frac{d\sigma_{3N}}{d\Omega_1} = |M_3^{fit}|^2 \int\int\int K p_3^2 dp_3 d\Omega_3 \ . \quad (13)$$

The phase-space integral extends beyond the detector limits to include the total recoil volume available at each θ_1 setting. Cross sections obtained using (13) are shown plotted in Fig. 12 (right-hand side), where the Legendre fit to $|M_3|^2$ was used to interpolate between the measured data points. A more conservative estimate of $d\sigma_{3N}$ is obtained by normalizing the purely phase-space portion of (13) (dashed line) to the angular region of the data where the average slope most closely follows phase space.

The total three-body cross section σ_{3N} was obtained as the integral over the fitted curves. The result was divided by 3! to account for the three identical protons. For the $|M_3^{fit}|^2$ curve we get

$$\sigma_{3N}(350 \text{ MeV}) = 1.80 \pm 0.07 \text{ mb}$$

and

$$\sigma_{3N}(500 \text{ MeV}) = 0.64 \pm 0.04 \text{ mb} \ .$$

Using the phase-space curve gives 1.53 ± 0.25 and 0.51 ± 0.07 mb, respectively. For each case the errors reflect only how well the fitted curve is determined statistically by the data. A summary of the two- and three-body cross sections (including normalization errors) extracted from this and other ^{3}He experiments is given in Table III and Fig. 13.

VI. DISCUSSION

Examination of Fig. 13 shows that while the overall strength and energy dependence of σ_{2N} is consistent with the quasideuteron interpretation near the (3,3) resonance, our data indicate a larger than expected σ_{2N} at higher energies. Below we discuss some of the possible explanations for this enhancement. Later, we discuss the three-body absorption results.

A. Binding effects

Table II shows that the number of deuterons N_d^{PWIA} required by the PWIA calculation to fit the data is smaller than the number N_d^{exp} obtained from simply scaling the free $\pi d \rightarrow pp$ cross sections as in Sec. IV, even though the PWIA uses the same $\pi d \rightarrow pp$ cross sections as input. This kinematic effect of the impulse approximation arises from the binding of the quasideuteron in the nucleus. The binding enhances the two-body absorption yield by shifting the effective interaction energy, and is particularly noticeable above the (3,3) resonance where the free

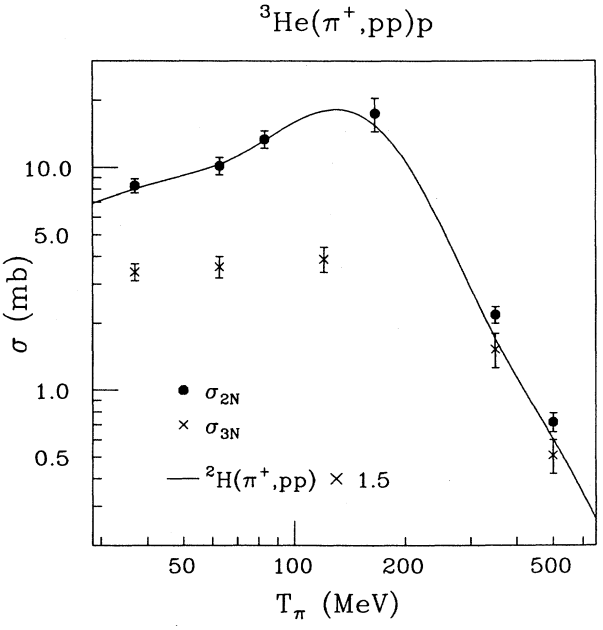

FIG. 13. Energy dependence of two-body and three-body pion absorption cross sections in ^{3}He. Solid line is parametrization of free $\pi d \rightarrow pp$ cross section (Ref. 28) multiplied by 1.5. References for previous measurements are given in Table III.

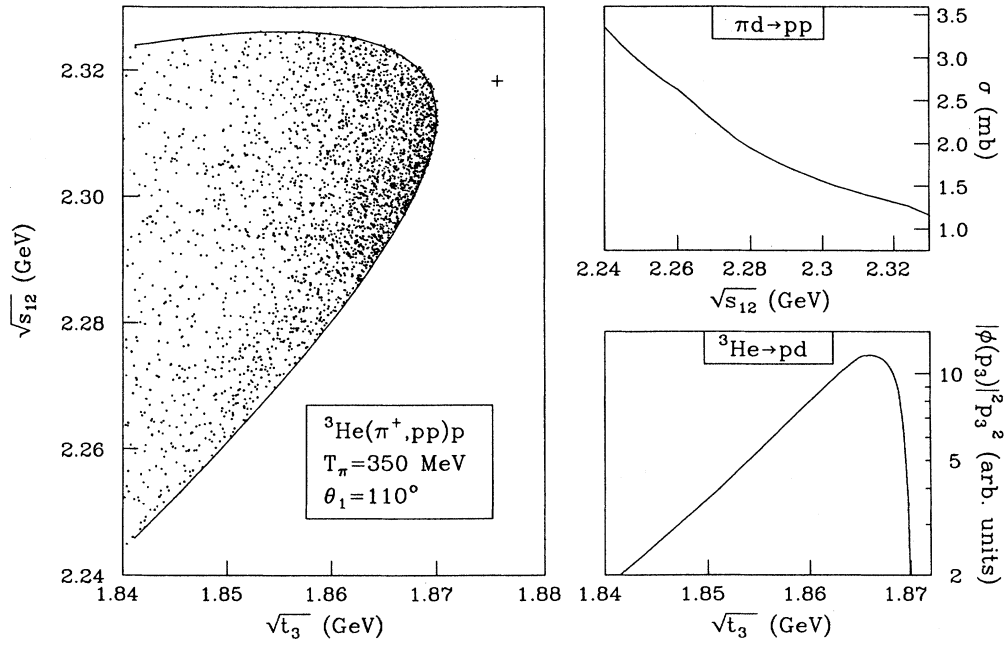

FIG. 14. Left: Chew-Low plot of physical region encompassing $^3He(\pi^+,pp)p$ reaction, showing distribution of measured events plotted versus quasideuteron mass $\sqrt{t_3}$ and c.m. energy $\sqrt{s_{12}}$ of detected protons p_1 and p_2. Symbol "+" denotes kinematic point of free $\pi d \rightarrow pp$ reaction. Right: relative (pd) momentum distribution (bottom) and energy dependence of $\pi d \rightarrow pp$ cross section (top) have largest effect on event density in Chew-Low plot according to impulse approximation.

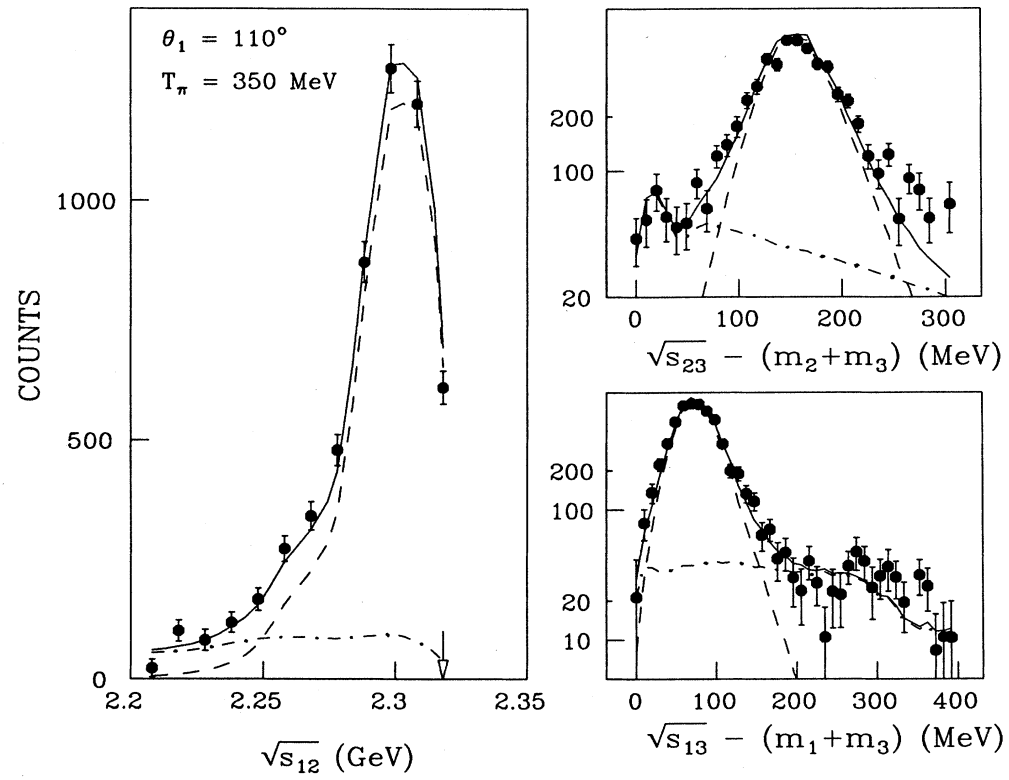

FIG. 15. Center-of-mass energy distributions of $^3He(\pi^+,pp)p$ yield at 350 MeV, $\theta_1=110°$. Arrow denotes c.m. energy corresponding to free $\pi d \rightarrow pp$ reaction. Curves have same meaning as in Figs. 8 and 9.

$\pi d \rightarrow pp$ cross section drops rapidly with energy.

Recall that under the impulse approximation the absorption matrix element $|M_{\pi d \rightarrow pp}|^2$ is calculated from the free cross section $d\sigma/d\Omega_1$, which is evaluated at a c.m. energy corresponding to the invariant mass s_{12} of the detected particles p_1 and p_2, where

$$s_{12}=(E_1+E_2)^2-(\mathbf{p}_1+\mathbf{p}_2)^2 . \quad (14)$$

Because of the Fermi motion of the bound deuteron, s_{12} does not coincide with the corresponding quantity s_{free} for a free deuteron, which is

$$s_{\text{free}}=(E_\pi+m_d)^2-p_\pi^2 . \quad (15)$$

Instead, for a fixed value p_3 of the recoil momentum, s_{12} ranges between s^+ and s^-, given by rewriting (14) as

$$s^{\pm}=(E_\pi+m_d^*)^2-(p_\pi \mp p_3)^2 , \quad (16)$$

where $m_d^*=m_d-\epsilon_b^*$ is the effective mass of the deuteron in ^{3}He arising from its nuclear binding energy $\epsilon_b^*=5.5+E_3-m_3$. These limits, which form the boundary of the physical region for the $^3\text{He}(\pi^+,pp)p$ reaction, correspond to the quasideuteron moving directly toward ($\cos\theta_3=1$) or away ($\cos\theta_3=-1$) from the pion. Because $m_d^*<m_d$, however, s_{12} will average out to be smaller than s_{free}. This energy shift can be interpreted loosely as resulting from the pion's loss of momentum and energy as a result of the breakup of ^{3}He into a free deuteron and a proton, whereupon the pion subsequently absorbs on the moving deuteron at a lower c.m. energy.[29]

The effect of the energy shift is illustrated using a Chew-Low diagram in Fig. 14 (left-hand side) where the physical region enclosed by the above limits on $\sqrt{s_{12}}$ is shown versus the mass of the quasideuteron. Within this region are plotted typical data at 350 MeV, for which the strong influence of $|M_2|^2$ is clearly seen. The event density, according to (10), is determined largely by the details of the nuclear wave function, but also by the energy dependence of the $\pi d \rightarrow pp$ reaction (Fig. 14, right-hand side). At 350 MeV the most probable value of $\sqrt{s_{12}}$ is calculated to occur some 20 MeV below $\sqrt{s_{\text{free}}}$ (denoted by the "+" in Fig. 14 and the arrow in Fig. 15), where the free $\pi d \rightarrow pp$ cross section is about 15% higher. This agrees with the experimental invariant mass distribution (Fig. 15), supporting the conclusion that binding effects are at least partially responsible for the observed enhancements in N_d above the (3,3) resonance.

B. Isovector absorption

At 500 MeV, the measured quasideuteron yield was larger than can be attributed to binding alone, and other effects must be considered. So far we have neglected the purely isovector reaction

$$\pi^+ + (pn)^1S_0 \rightarrow pp \; (T=1 \rightarrow I=1) , \quad (17)$$

which arises from the coupling of (pn) pairs to the singlet state in ^{3}He. Using the notation σ_{TI}, where T and I refer to the initial and final total isospin of the two nucleons,[30] we get from Clebsch-Gordon coupling

$$\sigma(\pi^+,pp)=1.5\sigma_{01}+0.25\sigma_{11} . \quad (18)$$

Assuming $\sigma_{01}=\sigma_{\pi d}$, any contribution from σ_{11} will cause an apparent increase in the number of deuterons N_d, ranging from 1.5 (for $\sigma_{11}=0$) to 1.75 or higher (for $\sigma_{11} \geq \sigma_d$).

The strength of the σ_{11} channel has been estimated independently from measurements of the asymmetry about $90^\circ_{\text{c.m.}}$ in $d\sigma/d\Omega$ that occurs in the reaction

$$\pi^- + (pp)^1S_0 \rightarrow pn \; (T=1 \rightarrow I=0,1) , \quad (19)$$

due to interference between the $I=0$ and $I=1$ amplitudes. Measurements[7,32] made below the (3,3) resonance determined that the cross section for reaction (19) is an order of magnitude smaller than $\sigma_{\pi d}$, because of a parity selection rule which forbids the reaction to proceed through an s-wave ΔN intermediate state. Furthermore, a partial-wave analysis of Piasetzky *et al.*[31] of the measured asymmetry found the ratio σ_{11}/σ_{10} to be less than 0.1. Using the relationship[30]

$$\sigma(\pi^-,pn)=0.5\sigma_{10}+0.25\sigma_{11} , \quad (20)$$

we get $\sigma_{11}/\sigma_{\pi d} \approx 0.02$. This indicates a negligible isovector contribution to quasideuteron absorption at low energies and is consistent with the value $N_d \approx 1.5$ measured there.

Piasetzky *et al.* point out that if d-wave pions were allowed, then the measured asymmetry in $d\sigma/d\Omega$ at 62.5 MeV would also be consistent with a larger value for the ratio σ_{11}/σ_{10}. Although d-wave contributions were negligible at the energy used in their analysis, both d and f waves must be appreciable at the energies of our measurement, as evidenced by the structure seen in the free $\pi d \rightarrow pp$ angular distributions. Analysis of $^3\text{He}(\pi^-,pn)$ data taken during this experiment is underway to determine whether the σ_{11} component is large enough to influence the (π^+,pp) yield.

C. Density effects

Most models of pion absorption predict some sensitivity to the radial shape of the two-nucleon wave function, due to the large mismatch between the required momentum transfer and that available from nuclear binding.[13,14] Thus, the increase in N_d at high bombarding energies could be due to the higher density of ^{3}He, compared to the deuteron. For example, if the form factor of the quasideuteron contains more high momentum components than does the physical deuteron, then we might expect the cross section to drop with bombarding energy slower for the quasideuteron than for the deuteron, especially at high energies where larger momentum transfer occurs.

Unfortunately, our understanding of the basic two-nucleon mechanism is poor in this energy region. Some studies have speculated that the one-pion-exchange model, which is fairly successful in explaining the $\pi d \rightarrow pp$ reaction near the (3,3) resonance, may compete at high energies with ρ-meson exchange or different processes entirely, such as single-nucleon absorption.[33] The absorption operator may no longer be dominated by excitation

of the Δ^{++} isobar at the pure $T=\frac{3}{2}\pi^+p\rightarrow\pi^+p$ scattering vertex, but include excitation of $T=\frac{1}{2}$ isobar as well.[34] If so, study of the quasifree ^{3}H(π^+,pp)n reaction would be worthwhile because the extra neutron might enhance this channel. Further studies of the high-energy quasideuteron yield in ^{3}He and ^{4}He are planned to understand the sensitivity of these processes to details of the (pn) relative wave function.[35]

D. Mechanisms for three-body absorption

Generally speaking, the enhanced event rate (relative to PWIA) seen in this experiment for recoil momenta above 200 MeV/c is a characteristic feature of all hadronic reactions on few-body systems. Although complex interactions among three hadrons would seemingly wash out any kinematic signatures and result in a more or less constant matrix element, there are exceptions. For example, in the knockout reactions[36] ^{2}H(p,2p)n and ^{3}He(p,pd)p, which also leave three hadrons in the final state, enhancement above phase space can be attributed to a low relative energy between various pairs of the emitted particles, where the strong s-wave elastic scattering cross sections lead to "soft" FSI effects. For the (π^+,pp) reaction, however, a high c.m. energy is favored for the detected proton pair, which reduces the likelihood of soft FSI between them. Although the recoil proton p_3 can have a low relative energy with respect to either p_1 or p_2, only a small fraction of the total phase space is occupied by such events.

We investigated FSI effects by rebinning the events according to the relative kinetic energy E_{13} and E_{23} between the spectator and each of the detected particles (where $E_{ij}=\sqrt{s_{ij}}-m_i-m_j$). A typical example from our 350-MeV absorption data is shown in Fig. 15 (right-hand side). Although the (pp) elastic scattering cross section varies by an order of magnitude over the plotted range of invariant energy, no radical departure from phase space is evident in the regions which lie outside the quasifree peak.

As noted earlier, the only variable for which the three-body absorption yield showed a significant departure from phase space was θ_1. The simplest mechanism that would involve this angle is a two-step initial-state interaction where the incoming pion transfers a large momentum to the first proton before absorbing on the remaining (pn) pair. The two protons emitted during the absorption step should display a forward peaked $\pi d\rightarrow pp$ angular distribution but centered around the direction of the *scattered* pion's momentum vector. Strong phase-space deviations should therefore occur at angle pairs (θ_1,θ_2) closest to the kinematics of quasifree knockout. This is consistent with the trend seen in our data, and might explain the minimum observed in $|M_3|^2$ at 90° lab, where kinematically we least expect to see the knocked-out proton. Large momentum transfers are particularly important since they lead to a smaller $\pi(pn)$ c.m. energy (and larger $\pi d\rightarrow pp$ cross section) for the scattered pion. Also, the knocked-out proton cannot receive sufficient momentum to exceed the detector thresholds unless it is emitted at forward angles. These factors may explain why the largest phase-space deviations occurred when either LAS or the TOF arm was at forward angles.

Masutani and Yazaki[37] have predicted that ISI effects should dominate pion absorption above the resonance. Laget[38] has calculated that the rescattering of on-shell pions makes a strong contribution to ^{3}H(π^+,pd) as well as to the three-body component of the ^{3}He(γ,pp)n and ^{3}He(γ,pn)p reactions. At present there is no theoretical estimate of ISI absorption of pions in ^{3}He, although calculations are planned.[39] It is reasonable, however, to expect the importance of ISI effects to scale with another channel to which it is strongly coupled—the quasifree knockout of two nucleons. The latter process, as noted earlier, was observed as a large background in our raw data. Also, the strong decrease of σ_{3N} with bombarding energy similar to that observed for σ_{2N} is consistent with a mechanism involving the on-shell $\pi d\rightarrow pp$ reaction.

Besides the largely on-shell ISI mechanism, which is sensitive only to the low-momentum part of the ^{3}He wave function, other contributions to three-body absorption may arise from multiple scattering of *off*-shell pions. Such processes are more sensitive to the small high-momentum components of the wave function and probably leave a less distinct kinematic signature in the differential distributions due to the more direct participation required by all three nucleons. Oset *et al.*[40] have calculated strong contributions to three-body absorption above the (3,3) resonance from diagrams containing direct and sequential (ΔN) interactions. Interestingly, such off-shell processes are much less important below the (3,3) resonance and contribute almost nothing at threshold. Table III shows the measured fraction $d\sigma_{3B}/(d\sigma_{2B}+d\sigma_{3B})$ at 350 MeV is indeed larger (by about 50%) than reported at 62.5 MeV. As it is particularly important to further establish the energy and isospin dependence of the three-body component, we are proceeding with our analysis of (π^+,pp) data taken at other energies, as well (π^-,pn) data taken during this experiment.

Summarizing, recoil momentum distributions of the ^{3}He(π^+,pp)p reaction were obtained at 350 and 500 MeV under kinematic conditions allowing separate observation of two- and three-body absorption. There is no obvious indication of interference between these two processes. The angular distribution of the two-body component follows closely the shape of the free $\pi d\rightarrow pp$ process. Comparison with a simple PWIA calculation shows good agreement between the theoretical and measured momentum distribution of the quasideuteron. However, an energy-dependent enhancement of the two-body yield is indicated, some of which may be due to the binding and form factor of the quasideuteron. Further study is underway to estimate the contribution from absorption on ($T=1$) (pn) pairs.

Three-body absorption cross sections were estimated from the coincidence data and account for at least 45% of the total absorption cross section, substantially larger than reported at lower energies. The origin of three-body absorption remains a mystery. The absence of any attenuation for the two-body component implies the three-body process is genuine (does not involve the two-body

directly). On the other hand, contributions from ISI cannot be ruled out, due to deviations from phase space seen in the angular distributions. Distributions obtained in other variables, however, showed no dramatic deviations from phase space. In particular, no evidence for FSI was seen. The energy dependence agrees with suggestions made by Oset that ΔN dynamics play an important role above the (3,3) resonance. Further experimental efforts should stress 4π detection, adequate statistics and good kinematic resolution to simplify the identification of specific mechanisms.

Cross sections published in this paper may be obtained from the first author (L.C.S.). A more detailed compilation will eventually be available in MENDLIB at LAMPF.

ACKNOWLEDGMENTS

This work is supported by the U.S. Department of Energy, Nuclear Physics Division, under Contract Nos. DEFG-0588-ER40390 and W-31-109-ENG-38, National Science Foundation and U.S.–Israel Binational Science Foundation.

[1]J. Favier *et al.*, Nucl. Phys. **A169**, 540 (1971); E. D. Arthur *et al.*, Phys. Rev. C **11**, 332 (1975); W. R. Wharton *et al.*, *ibid.* **31**, 526 (1985); R. Rieder *et al.*, *ibid.* **33**, 614 (1986); A. Altman *et al.*, *ibid.* **34**, 1757 (1986).

[2]D. Ashery and J. P. Schiffer, Annu. Rev. Nucl. Part. Sci. **36**, 207 (1986).

[3]W. R. Gibbs and W. B. Kaufmann, in *Pion-Nucleus Physics: Future Directions and Facilities at LAMPF,* Proceedings of the Los Alamos Conference on Pion-Nucleus Physics, AIP Conf. Proc. No. 163, edited by R. J. Peterson and D. D. Strottman (AIP, New York, 1987), p. 279.

[4]W. J. Burger *et al.*, Phys. Rev. Lett. **57**, 58 (1986).

[5]B. G. Ritchie, N. S. Chant, and P. G. Roos, Phys. Rev. C **30**, 969 (1984).

[6]A. Schumacher *et al.*, Phys. Rev. C **38**, 2205 (1988).

[7]S. Mukhopadhyay *et al.* (private communication).

[8]G. Backenstoss *et al.*, Phys. Rev. Lett. **55**, 2782 (1985).

[9]G. Backenstoss, Proceedings of the European Workshop on Few-Body Physics, Rome, 1986 [Few-Body Syst. Suppl. **1**, 516 (1986)].

[10]H. Ullrich *et al.*, Proceedings of the XIth European Conference on Few-Body Physics, Fontevraud, 1987 [Few-Body Syst. Suppl. **2**, 459 (1987)].

[11]K. A. Aniol *et al.*, Phys. Rev. C **33**, 1714 (1986).

[12]H. Hahn, M.Sc. thesis, Tel Aviv University, 1987.

[13]J. A. Niskanen and A. W. Thomas, Phys. Lett. B **196**, 299 (1987).

[14]K. Ohta, M. Thies, and T.-S. H. Lee, Ann. Phys. (N.Y.) **163**, 420 (1985).

[15]S. Homma and H. Tezuka, J. Phys. Soc. Jpn. **55**, 780 (1986).

[16]D. Ashery, Phys. Rev. C **36**, 460 (1987).

[17]J. Boswell *et al.*, Phys. Rev. C **32**, 1289 (1985).

[18]A. Klein *et al.*, Phys. Lett. B **187**, 253 (1987).

[19]I. S. Shapiro, Usp. Fiz. Nauk **92**, 549 (1967) [Sov. Phys.—Usp. **10**, 515 (1968)].

[20]S. Frullani and J. Mougey, *Advances in Nuclear Physics,* edited by J. W. Negele and E. Vogt (Plenum, New York, 1984), Vol. 14, pp. 81–84.

[21]H. Meier-Hajduk *et al.*, Nucl. Phys. **A405**, 581 (1983); **A395**, 332 (1983).

[22]C. Marchand *et al.*, Phys. Rev. Lett. **60**, 1703 (1988).

[23]M. Akemoto *et al.*, Phys. Lett. **149B**, 321 (1984); M. Ja. Borkowski *et al.*, J. Phys. G **11**, 69 (1985); J. Boswell *et al.*, Phys. Rev. C **25**, 2540 (1982); R. M. Heinz *et al.*, Phys. Rev. **167**, 1232 (1968).

[24]E. Coltun, Nucl. Instrum. Methods **178**, 95 (1980).

[25]K. L. Brown and Ch. Iselin, CERN Report 74-2, 1974.

[26]R. Madey *et al.*, Nucl. Instrum. Methods **214**, 401 (1983).

[27]L. Orphanos *et al.*, Phys. Rev. C **26**, 2111 (1982).

[28]J. Bystricky *et al.*, J. Phys. (Paris) **48**, 1901 (1987).

[29]P. C. Gugelot, Phys. Rev. C **30**, 654 (1984).

[30]D. Ashery *et al.*, Phys. Rev. Lett. **47**, 895 (1981).

[31]E. Piasetzky *et al.*, Phys. Rev. Lett. **57**, 2135 (1987).

[32]M. A. Moinester *et al.*, Phys. Rev. Lett. **52**, 1203 (1984); G. Backenstoss *et al.*, Phys. Lett. **137B**, 329 (1984).

[33]B. D. Keister and L. S. Kisslinger, Nucl. Phys. **A326**, 445 (1979).

[34]R. Bertini *et al.*, Phys. Lett. **162B**, 77 (1988).

[35]L. C. Smith and R. C. Minehart, LAMPF Proposal for Experiment 1126, 1988.

[36]T. R. Whitten *et al.*, Nucl. Phys. **A254**, 269 (1973); R. D. Felder *et al.*, *ibid.* **A280**, 308 (1977); Bracco *et al.*, Phys. Lett. **137B**, 311 (1984).

[37]K. Masutani and K. Yazaki, Nucl. Phys. **A407**, 309 (1983).

[38]J. M. Laget, Phys. Rev. C **35**, 832 (1987); J. Phys. G **14**, 1445 (1988).

[39]J. M. Laget (private communication).

[40]E. Oset *et al.*, Nucl. Phys. **A448**, 597 (1986).